Enhanced pyrite passivation by carrier-microencapsulation using Fe-catechol and Ti-catechol complexes

Xinlong Li [a,*,1], Ilhwan Park [b,*,1], Carlito Baltazar Tabelin [c], Kosuke Naruwa [a], Taiki Goda [a], Chie Harada [a], Sanghee Jeon [b], Mayumi Ito [b], Naoki Hiroyoshi [b]

[a] Division of Sustainable Resources Engineering, Graduate School of Engineering, Hokkaido University, Japan

[b] Division of Sustainable Resources Engineering, Faculty of Engineering, Hokkaido University, Japan

[c] School of Minerals and Energy Resources Engineering, The University of New South Wales, Sydney, NSW 2052, Australia

* Corresponding author. E-mail address: rikinryu@gmail.com (X. Li), i-park@eng.hokudai.ac.jp (I. Park)

[1] These authors contributed equally to this work.

Abstract

Acid mine drainage (AMD) formation is mainly caused by the oxidation of pyrite. Carrier-microencapsulation (CME) using metal-catecholate complexes has been proposed to passivate sulfide minerals by forming surface-protective coatings on their surfaces. Among the various metal-catecholate complexes, Ti-catecholate formed stable coatings having superior acid-resistance, but a thick enough passivating film required considerable time (ca. 14 days) to grow. Meanwhile, Fe-catecholates can form Fe-oxyhydroxide coatings within 2 days, however, they are less stable than Ti-based coating. To address these drawbacks of using a single metal-complex, this study investigated the concurrent use of Fe-catechol and Ti-catechol complexes for accelerating the formation of stable passivating coating on pyrite.

Compared with a single metal-complex system, the coating formation was significantly accelerated in mixed system. Linear sweep voltammetry showed the simultaneous decomposition of $[Fe(cat)]^{+}$ and $[Ti(cat)_3]^{2-}$ as the

main reason for improved coating formation. Electrochemical properties of coatings formed by single and mixed complex systems, confirmed by electrochemical impedance spectroscopy and cyclic voltammetry, indicated the coating formed in the mixed system had higher resistance and more electrochemically inert than the other cases. The simultaneous use of Fe-catechol and Ti-catechol complexes enhanced pyrite passivation by accelerating metal-complex decomposition and forming more stable coating composed of Fe_2TiO_5.

Keywords: acid mine drainage; pyrite; carrier-microencapsulation; Fe-catecholate complex; Ti-catecholate complex

1. Introduction

Mining and mineral processing industries are essential for metal production and often generate large amounts of sulfide-rich wastes, which are known to generate acid mine drainage (AMD) when exposed to the environment (Johnson and Hallberg, 2005; Park et al., 2019, 2020a; Tabelin 2017a, 2017b, 2020a; Tomiyama et al., 2019, 2020). Similarly, huge amounts of sulfide-bearing soils, sediments and rocks are being excavated from underground space development for modern railways and road system, powerplants, shopping malls and parking spaces, and radioactive waste repositories, which have been reported to generate AMD-like and highly contaminated effluents (Huyen et al., 2019a, 2019b; Ho et al., 2021; Li et al., 2016; Tabelin et al., 2012a, 2012b, 2014a, 2014b; Tamoto et al., 2015). Among all sulfide minerals, pyrite (FeS_2) is the primary cause of AMD formation because it is the most common and abundant in nature (Tabelin et al., 2018).

Acid mine drainage is not only acidic but also highly contaminated with heavy metals (e.g., cadmium (Cd), copper (Cu), iron (Fe), manganese (Mn), lead (Pb), and zinc (Zn)) (Igarashi et al., 2020; Tabelin and Igarashi, 2009; Tabelin et al., 2013, 2017c, 2017d; Tatsuhara et al., 2013) and toxic metalloids like arsenic (As) and selenium (Se) (Opiso et al., 2021; Tabelin et al., 2010, 2012c, 2014c), and is considered one of the most serious environmental problems encountered by mining and mineral processing industries worldwide. If released to the environment without appropriate treatments, AMD could seriously damage the surrounding water bodies, soil and sediment systems, and ecosystems. To manage AMD, the most commonly used strategy is chemical neutralization whereby basic materials like limestone ($CaCO_3$), quicklime (CaO) or slaked lime ($Ca(OH)_2$) are mixed with AMD to raise its pH to precipitate-immobilize almost all toxic and hazardous metal(loid) ions as metal-oxyhydroxides (Park et al., 2019; Tabelin et al., 2021a). Although neutralization-based remediation is very effective to mitigate the negative environmental impacts of AMD, it has two critical drawbacks: (1) almost perpetual treatment is

required because AMD formation typically lasts for several hundreds or even thousands of years (Davis Jr. et al., 2000; Tabelin et al., 2019a), and (2) disposal of huge amounts of bulky and hazardous sludge produced by the treatment (Gazea et al., 1996; Kefeni et al., 2015; Park et al., 2020b; Taylor et al., 2005).

Due to the above-mentioned limitations of neutralization, one promising alternative strategy to limit AMD formation is by directly passivating sulfide minerals with surface-protective layers in a process generally referred to as microencapsulation. Several microencapsulation techniques have been developed in recent years to coat pyrite with inorganic-based (e.g., ferric oxyhydroxides/oxides, ferric phosphate and ferric silicates) (Evangelou, 1995; Huminicki and Rimstidt, 2009; Zhang and Evangelou, 1998), organic-based (e.g., humic acids, triethylenetetramine (TETA), lipids) (Ačai et al., 2009; Cai et al., 2005; Elsetinow et al., 2003), and hybrid inorganic/organic-based coatings (e.g., methyltrimethoxysilane (MTMOS), n-propyltrimethoxysilane (NPS), γ-mercaptopropyltrimethoxysilane (PropS-SH)) (Diao et al., 2013; Khummalai and Boonamnuayvitaya, 2005; Ouyang et al., 2015). These encapsulation techniques passivated sulfide minerals like arsenopyrite (FeAsS) and pyrite; however, they were either non-selective (i.e., cannot target the 1–10% of sulfide minerals found in mining wastes) or biologically degradable in the environment.

To address these limitations, carrier-microencapsulation (CME) was developed by the authors (Satur et al., 2007). This technique uses redox-sensitive metal-organic complexes—sparingly soluble metal ions like aluminum (Al^{3+}), iron (Fe^{3+}), and titanium (Ti^{4+}) together with an organic complexing agent like catechol (1,2-dihydroxybenzene, $C_6H_4(OH)_2$)—that specifically decompose on minerals when they undergo electrochemical dissolution (Li et al., 2019a; Park et al., 2018a, 2018b). As a result of the complex decomposition, metal ions are released and precipitated as metal-oxyhydroxides/oxides on the mineral surface. Once pyrite is coated with metal-oxyhydroxides/oxides, interactions of dissolved oxygen (DO), ferric ion (Fe^{3+}), water and the mineral surface are inhibited, suppressing sulfide dissolution (Eqs. 1–3).

$$2FeS_{2(s)} + 7O_{2(aq)} + 2H_2O \rightarrow 2Fe^{2+}_{(aq)} + 4SO_4^{2-}{}_{(aq)} + 4H^{+}_{(aq)} \quad (1)$$

$$4Fe^{2+}_{(aq)} + O_{2(aq)} + 4H^{+}_{(aq)} \rightarrow 4Fe^{3+}_{(aq)} + H_2O \quad (2)$$

$$FeS_{2(s)} + 14Fe^{3+}_{(aq)} + 8H_2O \rightarrow 15Fe^{2+}_{(aq)} + 2SO_4^{2-}{}_{(aq)} + 16H^{+}_{(aq)} \quad (3)$$

Among the metal-catecholate complexes previously evaluated by the authors for CME, Ti-catecholate complex was the most promising due to the high stability of coating formed even under acidic conditions. Park et

al. (2018a), for example, confirmed the oxidative decomposition of Ti-catecholate complex ($[Ti(cat)_3]^{2-}$) and arsenopyrite/pyrite coating with TiO_2, which was stable in the pH range of 3–12. CME has been proposed for application during flotation before tailings are disposed into tailings storage facility (TSF) because directly introducing Ti-catecholate complex into the acidic environment of TSFs would destabilize metal-catecholate complexes and limit its effectiveness (Park et al., 2021). Flotation—the most commonly used technique to produce saleable concentrates (Aikawa et al., 2019; Hornn et al., 2020a, b; Tabelin et al., 2021b)—is typically operated under neutral to alkaline conditions (i.e., pH > 7) to depress non-valuable sulfide minerals like pyrite, which makes the application of CME to flotation tailings more practical. Although Ti-based CME can passivate pyrite present in flotation tailings, there is an apparent limitation on its applicability due to the sluggish decomposition of Ti-catecholate complex (Park et al., 2018a). Other types of metal-catecholate complexes like $[Al(cat)]^+$ and $[Fe(cat)]^+$ have faster reaction kinetics for coating formation (< 2 days), but the coatings they formed were less stable than that of Ti-based CME (Li et al., 2019a; Park et al., 2018a, 2018b, 2019).

Thus, the accelerated formation of stable coating remains a challenge to be solved in CME. To meet this need, the present study examined CME treatment of pyrite using two different types of complexes (i.e., Fe-catechol and Ti-catechol complexes) with the aims of not only creating more stable coating composed of Fe—Ti—O than Fe-oxyhydroxide formed by Fe-based CME but also accelerating coating formation process compared to Ti-based CME. The specific objectives of this study are three-fold: (1) to identify the stabilities of Fe-catechol and Ti-catechol mixtures, (2) to investigate the complex decomposition/coating formation occurring in the presence of pyrite, and (3) to evaluate the properties of coatings formed by Fe-catechol and Ti-catechol complexes. The first objective was clarified by ultraviolet-visible (UV-vis) light spectrophotometry while the second and third objectives were achieved by batch-type leaching experiments, surface characterization of residues using X-ray photoelectron spectroscopy (XPS), and electrochemical studies (e.g., linear sweep voltammetry (LSV), cyclic voltammetry (CV), and electrochemical impedance spectroscopy (EIS)).

2. Materials and methods

2.1. Stabilities of Fe-catechol and Ti-catechol complexes

To check the stabilities of Fe-catechol and Ti-catechol complexes in mixed systems, solutions containing 1 mM Fe^{3+}, 1 mM Ti^{4+}, and various concentrations of catechol (0–6 mM) were prepared using ferric nitrate nonahydrate ($Fe(NO)_3 \cdot 9H_2O$), high purity (99.9%) Ti standard solution for ICP-AES (1000 mg/L Ti^{4+} in 1 M

H_2SO_4), and pyrocatechol. After adding Fe^{3+}, Ti^{4+} and catechol (cat) into deionized (DI) water (18 MΩ cm, Milli-Q® Integral Purification System, Merck Millipore, USA), solutions were magnetically stirred at 200 rpm under ambient conditions, their pH was adjusted to 8.0 ± 0.1 using dilute HNO_3 and NaOH, and then allowed to stabilize for 10 min. The pH 8 was chosen because CME has been proposed for treating flotation tailings (pH > 7). At pH greater than 7, two types of Fe-catecholate complexes can be formed (i.e., $[Fe(cat)_2]^-$ at pH < 9 and $[Fe(cat)_3]^{3-}$ at pH > 9); however, between two complexes, only the former can create the surface protective coating on pyrite (Li et al., 2019a). Because of this, pH 8 was selected not only to synthesize $[Fe(cat)_2]^-$ selectively but also to avoid the formation of $[Fe(cat)_3]^{3-}$. After this, solutions were filtered through 0.2 μm syringe-driven membrane filters (LMS Co. Ltd., Japan) to remove precipitates and polymerized organic molecules, and filtrates were immediately analyzed by atomic emission spectrometer (ICP-AES, ICPE 9820, Shimadzu Corporation, Japan) and UV-vis spectrophotometer (V-630, Jasco Analytical Instruments, Japan) in a single-crystal quartz cell between 350 and 800 nm. For UV-vis measurements, Fe-Ti-cat solutions were diluted 10 times (i.e., 0.1 mM Fe^{3+} and Ti^{4+} with 0.1–0.6 mM catechol).

2.2. CME treatments of pyrite with Fe-catechol and Ti-catechol complexes

The pyrite sample used in this study was obtained from Cerro de Pasco mine, Peru. It was primarily crush ed by a hammer down to about 2 cm in diameter and hand picking was conducted to remove the visible impurities. Afterwards, the crushed pyrite sample was further crushed by a jaw crusher (BB 51, Retsch Inc., Germany), ground by a vibratory disc mill (RS 100, Retsch Inc., Germany), and screened to obtain a size fraction between 106 and 150 μm in diameter. Prior to the experiments, pyrite sample was washed using the method developed by McKibben and Barnes (1986) to remove slime coatings as well as any oxidized layer formed during sample preparation and storage. This washing method involves ultrasonic desliming in ethanol, washing with 1 M HNO_3, rinsing with DI water, dewatering with acetone, and drying in a vacuum desiccator.

Three types of solutions were prepared for CME treatment: (i) 5 mM Fe^{3+} and 30 mM catechol, (ii) 5 mM Ti^{4+} and 30 mM catechol, and (iii) 5 mM Fe^{3+}, 5 mM Ti^{4+} and 30 mM catechol. The pH of solution was fixed to 8.0 where both Fe-catechol and Ti-catechol complexes are stable. One gram of washed pyrite and 10 mL of solution were put in a 50-mL Erlenmeyer flask and shaken in a constant temperature water bath (25°C) at 120 strokes/min under oxic conditions. At predetermined time intervals, the suspensions were filtered through 0.2 μm syringe-driven membrane filters, then the filtrates were analyzed by ICP-AES. Meanwhile, the residue was

thoroughly washed with DI water, dried in a vacuum oven at 40°C for 1 day, then analyzed by XPS (JPS-9200, JEOL Ltd., Japan) to characterize the surface of pyrite after CME treatment. The XPS analysis was conducted using an Al Kα X-ray source (1486.7 eV) operated at 100 W (voltage = 10 kV; current = 10 mA) under ultrahigh vacuum conditions (~6.7×10^{-7} Pa). The collected XPS spectra were processed using CasaXPS software (version 2.3.23).

2.3. Electrochemical studies

Oxidative decompositions of complexes in single and mixed complex systems were investigated by anodic linear sweep voltammetry (LSV) using a computer-controlled electrochemical measurement unit (SI 1280B, Solartron Instruments, UK). A conventional three-electrode system, consisting of a platinum (Pt) rod working electrode, a Pt wire counter electrode, an Ag/AgCl reference electrode filled with 3.3 M NaCl, was used in this study. A water-jacket type glass cell was connected to a recirculating thermostat water bath (BB400, Yamato Scientific Co. Ltd., Japan). Three types of solutions containing (i) 1 mM Fe^{3+} and 3 mM catechol, (ii) 1 mM Ti^{4+} and 3 mM catechol and (iii) 1 mM Fe^{3+}, 1 mM Ti^{4+} and 6 mM catechol were prepared for LSV measurement. All solutions contained 0.1 M $NaNO_3$ as supporting electrolyte and their pH was adjusted to 8 using dilute NaOH. 12 mL of prepared solution was poured in the cell maintained at 25°C and deoxygenated by purging with N_2 (99.999% purity) for 30 min through a Teflon® tube. The position of tube tip was adjusted slightly above the surface of the solution prior to each experiment, and N_2 was continuously introduced into the cell to keep an anoxic atmosphere during the measurement. The LSV measurement commenced after equilibration at the open circuit potential (OCP) at a sweep rate of 5 mV/s up to +0.8 V.

For the comparison of coatings formed by Fe-catechol complex with and without Ti-catechol complex, the Pt electrode was pretreated by chronoamperometry at +0.8 V for 1 h in solutions containing (i) 5 mM Fe^{3+} and 15 mM catechol, and (ii) 5 mM Fe^{3+}, 5 mM Ti^{4+} and 30 mM catechol to induce the coating formation. A Pt electrode was used as a working electrode to evaluate the electrochemical properties of different coatings properly without interference from pyrite. After this, the pretreated electrode was taken out from the solution, washed with DI water, and then used as working electrode for electrochemical impedance spectroscopy (EIS), which was operated under the following conditions: DC bias, 0 V vs OCP; AC amplitude, 5 mV; AC frequency, 20,000 Hz to 0.1 Hz; electrolytes, dilute H_2SO_4 solution (pH 2.5). Moreover, cyclic voltammetry (CV) of pretreated electrode was carried out to evaluate redox properties of coatings. For CV measurements, the pretreated electrode was immersed

in deoxygenated 0.1 M $NaNO_3$ solution, equilibrated at OCP, and then measured between –0.8 to +0.8 V at a scan rate of 5 mV/s. The scan direction was towards more negative potentials first (i.e., cathodic direction) because Fe^{III} species in coatings cannot be further oxidized.

3. Results and discussion

3.1. CME treatment using Fe-catechol and Ti-catechol complexes

Figure 1a shows the concentrations of Ti^{4+} and Fe^{3+} in solutions containing various concentrations of catechol at pH 8. Without catechol, both Ti^{4+} and Fe^{3+} were precipitated, but with catechol, their concentrations increased as the concentration of catechol increased. The higher solubilities of Ti and Fe could be attributed to the formation of metal-catecholate complexes with the appropriate number of catechol ligands. As shown in UV-vis spectra (Fig. 1b), two absorption bands were observed at around 380 and 580 nm, corresponding to the presence of $[Ti(cat)_3]^{2-}$ and $[Fe(cat)_2]^{-}$, respectively (Li et al., 2019a; Park et al., 2018a). It is interesting to note that although both complexes can coexist, the formation of $[Ti(cat)_3]^{2-}$ is more preferable at low concentration of catechol (1 mM) than that of $[Fe(cat)_2]^{-}$ (Fig. 1a). At higher concentrations of catechol, both Ti^{4+} and Fe^{3+} concentrations increased, reaching 0.95 mM and 0.81 mM, respectively, at 6 mM catechol. Based on this result, Fe-Ti-cat solution was prepared at the ratio of 1:1:6 to synthesize stable Fe- and Ti-catecholate complexes for CME treatment.

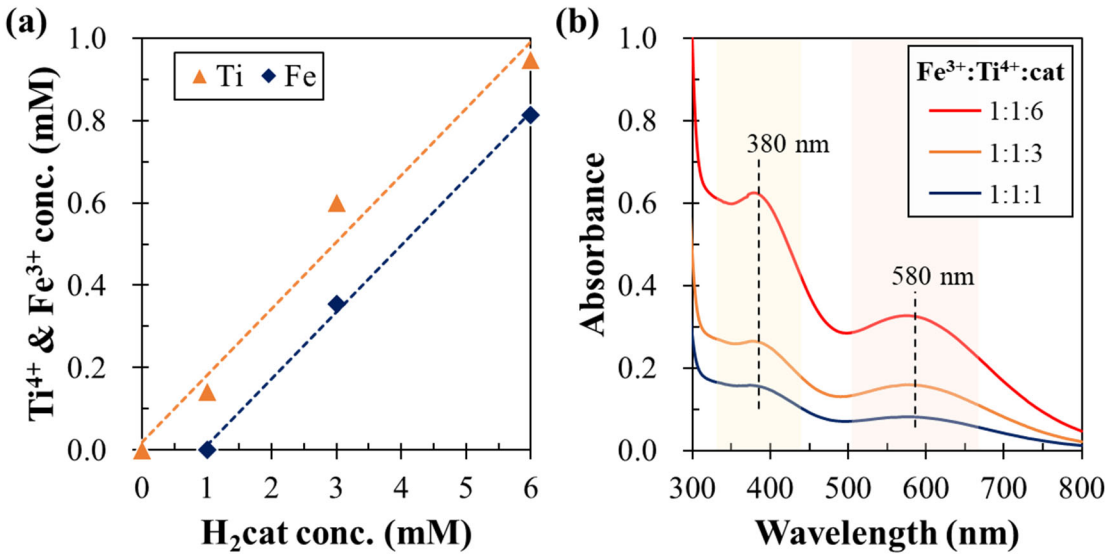

Fig. 1. Effects of molar ratio of catechol to metal ions on the formation of Fe-catechol and Ti-catechol complexes: (a) dissolved Ti and Fe concentrations, and (b) UV-vis spectra.

To investigate the effects of Fe-catechol and Ti-catechol complexes on coating formation during CME treatment of pyrite, batch-type leaching experiments were conducted (Fig. 2). For comparison, CME treatments of pyrite in single complex systems—Fe-catechol only or Ti-catechol only—were also conducted as "controls". Figure 2a shows the changes in dissolved Fe concentration with time. When only Fe-catecholate complex was present, dissolved Fe concentration gradually decreased with time and after 7 days, its concentration decreased by 60%. This decrease in dissolved Fe concentration likely occurred via sequential decomposition of $[Fe(cat)_2]^-$ (i.e., $[Fe(cat)_2]^- \rightarrow [Fe(cat)]^+ \rightarrow Fe^{3+}$; Eqs. (4) and (5)), followed by precipitation of Fe^{3+} (Eq. (6).

$$[Fe(cat)_2]^- + 2H^+ + 1/2O_2 = [Fe(cat)]^+ + Q + H_2O \quad (4)$$

$$[Fe(cat)]^+ + 2H^+ + 1/2O_2 = Fe^{3+} + Q + H_2O \quad (5)$$

$$Fe^{3+} + 3H_2O = Fe(OH)_3 + 3H^+ \quad (6)$$

where Q is ortho-quinone (1,2-benzoquinone, $C_6H_4O_2$), an oxidation product of catechol. In the case when two complexes coexisted, dissolved Fe concentration decreased rapidly; that is, after 4 days, Fe^{3+} concentration decreased by around 98% in Fe-Ti-catechol system (Fig. 2a).

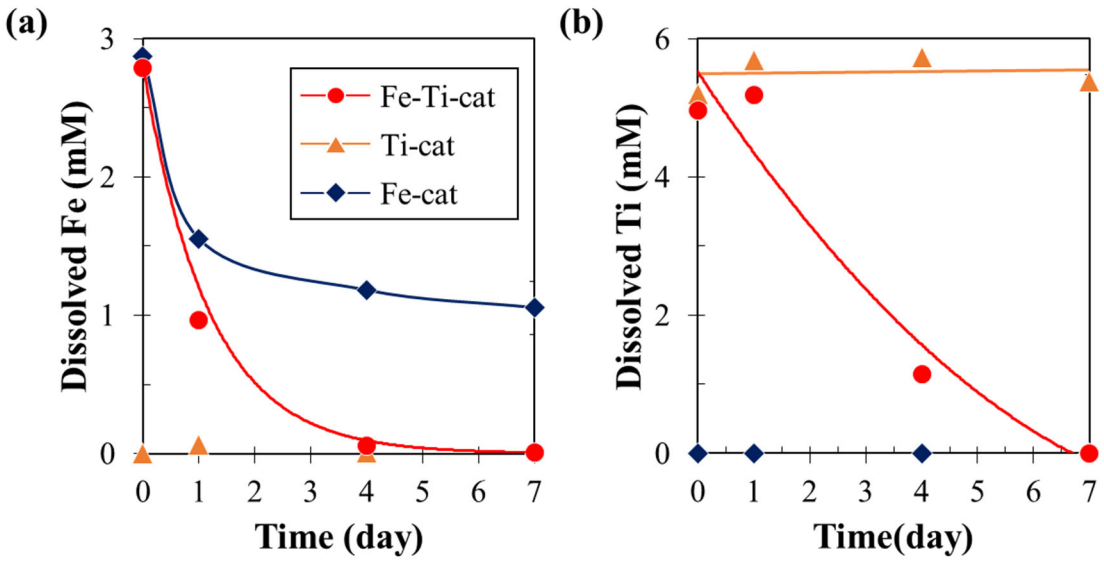

Fig. 2. CME treatments for pyrite in single (Fe-catechol or Ti-catechol) and mixed complex (Fe-Ti-catechol) systems: (a) dissolved Fe and (b) dissolved Ti concentrations with time.

Similarly, the decrease in dissolved Ti concentration was only achieved when two complexes were present (Fig. 2b). Park et al. (2018a) reported that Ti-catecholate complex is very stable, so it requires ca. 25 days for almost all the complexes to be decomposed on arsenopyrite surface. However, around 99% of dissolved Ti was precipitated within 7 days in Fe-Ti-catechol system, indicating Fe-catecholate complex catalyzed Ti-catecholate complex decomposition and coating formation (Eqs. 7 and 8).

$$[Ti(cat)_3]^{2-} + 6H^+ + 3/2O_2 = Ti^{4+} + 3Q + 3H_2O \quad (7)$$

$$Ti^{4+} + 4H_2O = Ti(OH)_4 + 4H^+ \quad (8)$$

After 7-day treatments of pyrite in Fe-cat, Ti-cat, and Fe-Ti-cat systems, the residues were analyzed by XPS to characterize the nature of coating formed (Fig. 3). The XPS Ti 2p spectra of pyrite treated with Ti-cat and Fe-Ti-cat (Fig. 3a) showed two peaks of Ti^{4+} corresponding to Ti $2p_{1/2}$ and Ti $2p_{3/2}$ at 464.0 and 458.4 eV, which indicate the existence of the Ti^{4+} oxidation state on their surfaces (An et al., 2017; Bahareh and Habibi, 2019; Regue et al., 2020). Meanwhile, deconvolution of Fe $2p_{3/2}$ spectra of pyrite treated with Fe-cat, Ti-cat, and Fe-Ti-cat (Fig. 3b) illustrated the various Fe coordination and oxidation states present on their surfaces: (i) Fe^{II}—S of pyrite (706.9 eV) (Nesbitt and Muir, 1994; Qui et al., 2013; Tabelin et al., 2019b), (ii) Fe^{III}—S of partially oxidized pyrite (709.0 eV) (Nesbitt and Muir, 1994; Tabelin et al., 2019b), (iii) Fe^{III}—O of Fe-oxyhydroxides (713.2 and 711.0 eV) (Grosvenor et al., 2004; Nesbitt and Muir, 1994; Park et al., 2021; Tabelin et al., 2019b), and (iv) Fe^{III}—SO_4 (714.6 eV) (Park et al., 2021; Tabelin et al., 2020b). As shown in Fig. 3b, all treated pyrite samples showed strong signals of Fe-oxyhydroxides, which can be formed due to pyrite oxidation and/or the decomposition of Fe-catecholate complex. The total percentage of Fe^{III}—O in the Fe $2p_{3/2}$ spectra of pyrite treated with Fe-cat, Ti-cat, and Fe-Ti-cat were about 80%, 55%, and 70%, respectively, which indicate that the presence of Fe-catecholate complex facilitated the formation of Fe-oxyhydroxide on the surface of pyrite. Meanwhile, the Fe $2p_{3/2}$ spectrum of pyrite treated with Ti-cat and Fe-Ti-cat showed an additional peak at about 712.3 eV, which is assigned to Fe^{III}—Ti—O (An et al., 2017; Bahareh and Habibi, 2019; Regue et al., 2020). The presence of both Ti^{4+} (Fig. 3a) and Fe^{III}—Ti—O (Fig. 3b) implies that pyrite is most likely coated with $Fe^{III}_2Ti^{IV}O_5$. Lee et al. (2020) also reported that Fe_2TiO_5 can be synthesized electrochemically using Fe-catechol and Ti-catechol complexes. The formation of Fe—Ti—O coating was further confirmed by SEM-EDS of Pt electrode pretreated with Fe-catechol and Ti-catechol complexes (Fig. S1). As can be seen in Ti 2p spectra (Fig. 3a), the intensities of Ti^{4+} observed in Fe-Ti-cat are significantly stronger (i.e., 3.5 times) than those in Ti-cat case. This indicates that more Fe_2TiO_5 coating

was formed when the two complexes coexisted, which is in line with the results of ICP-AES analysis (Fig. 2). Moreover, the formation of Fe_2TiO_5 by $[Ti(cat)_3]^{2-}$ and $[Fe(cat)_2]^-$ are thermodynamically favorable because the standard Gibbs free energy change (ΔG^0) of Eq. (9) calculated based on thermodynamic data listed in Table 1 was –126.8 kJ/mol.

$$2[Fe(cat)_2]^- + [Ti(cat)_3]^{2-} + 4H^+ + 7/2O_2 \rightarrow Fe_2TiO_5 + 7Q + 2H_2O \quad (9)$$

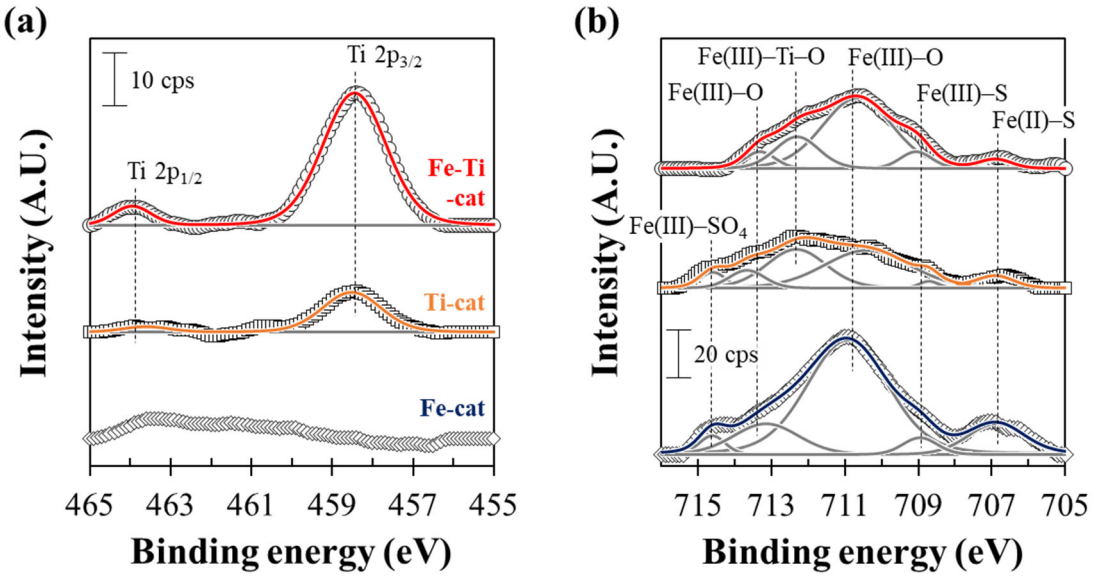

Fig. 3. XPS analysis of pyrite treated by Fe-cat, Ti-cat, and Fe-Ti-cat systems: (a) Ti 2p and (b) Fe $2p_{3/2}$ spectra.

Table 1. Standard Gibbs free energy of formation (ΔG^0_f) used in this study.

Component	$\Delta G^0_{f\,(kJ/mol)}$	Reference
H^+	0	Dean and Lange (1999)
O_2	0	Dean and Lange (1999)
H_2O	–237.1	Dean and Lange (1999)
H_2cat	–210.0	Dean and Lange (1999)
Q	–56.6	Horner and Geyer (1965)[*1]
$[Fe(cat)_2]^-$	–198.1	Avdeef et al. (1978)[*2]
$[Ti(cat)_3]^{2-}$	–342.5	Creutz and Chou (2008)[*2]
Fe_2TiO_5	+4.9	Kumagai et al. (2018)

*1 ΔG^0_f of Q was calculated from standard electrode potential of Q/H_2cat reported in Horner and Geyer (1965) and ΔG^0_f of catechol.

*2 ΔG^0_f of $[Fe(cat)_2]^-$ was calculated from the stability constants determined by experiments by Avdeef et al. (1978). ΔG^0_f of $[Ti(cat)_3]^{2-}$ was calculated by the constant reported by Creutz and Chou (2008).

To verify the detailed mechanisms of how Fe-catechol and Ti-catechol complexes are oxidatively decomposed in Fe-Ti-cat system and how the coexistence of two complexes accelerated their decompositions, electrochemical properties of Fe-cat, Ti-cat, and Fe-/Ti-cat complexes under oxidizing conditions were investigated by LSV (Fig. 4). As shown in the linear sweep voltammogram of Ti-catechol solution, there is an anodic peak (i.e., A_1) observed at around 0.5 V, which corresponds to the oxidative decomposition of $[Ti(cat)_3]^{2-}$ as follows:

$$[Ti(cat)_3]^{2-} \rightarrow Ti^{4+} + 3Q + 6e^- \quad (10)$$

LSV of Fe-catechol solution shows two anodic peaks at 0.30 V (A^*_1) and 0.46 V (A^*_2). At pH 8, the dominant species is $[Fe(cat)_2]^-$, so the first anodic peak (A^*_1) is considered as the oxidation of $[Fe(cat)_2]^-$ to $[Fe(cat)]^+$ (Eq. 11). Afterwards, with increasing potential, $[Fe(cat)]^+$ undergoes the oxidation process until all catechol molecules coordinated with Fe^{3+} are oxidatively decomposed (Eq. 12).

$$[Fe(cat)_2]^- \rightarrow [Fe(cat)]^+ + Q + 2e^- \quad (11)$$

$$[Fe(cat)]^+ \rightarrow Fe^{3+} + Q + 2e^- \quad (12)$$

When Fe-catechol and Ti-catechol complexes coexisted in the solution, both A^*_1 and A^*_2 peaks appeared almost at the same potential as observed in LSV of Fe-catechol solution; however, an anodic peak of $[Ti(cat)_3]^{2-}$ (A_1) disappeared. Moreover, it is important to note that the current density of A^*_2 was substantially increased. This increase in the current density of A^*_2 could be speculated that $[Fe(cat)]^+$ and $[Ti(cat)_3]^{2-}$ were decomposed together (Eq. 13), indicating that the former enhanced the latter's decomposition reaction, and thus the precipitation of Fe^{3+} and Ti^{4+} were accelerated when they coexisted (Figs. 2–4).

$$[Fe(cat)]^+ + [Ti(cat)_3]^{2-} \rightarrow Fe^{3+} + Ti^{4+} + 4Q + 8e^- \quad (13)$$

Based on the results of leaching tests, XPS analysis, and LSV, it can be deduced that coexistence of Fe-catechol and Ti-catechol complexes accelerated coating formation due to the change in oxidative decomposition process of Ti-catecholate complex, which is simultaneously decomposed with $[Fe(cat)]^+$ (Figs. 2 and 4) and creates the coating composed of Fe—Ti—O (Fig. 3).

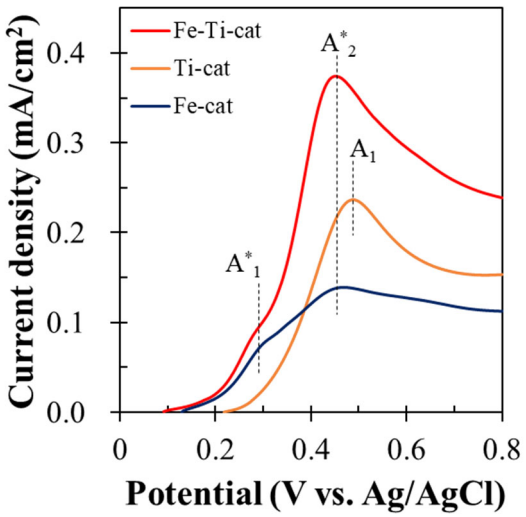

Fig. 4. Linear sweep voltammograms of Fe-cat, Ti-cat, and Fe-Ti-cat solutions at pH 8.

3.2. Electrochemical property of coating formed by Fe-catechol and Ti-catechol complexes

Electrochemical impedance spectroscopic analysis was conducted to evaluate the properties of coatings formed in solutions containing Fe-cat and Fe-Ti-cat complexes. These two systems were chosen because they could form coatings during CME treatment for pyrite as confirmed in Fig. 2. In addition, EIS was also conducted using Pt electrode pretreated in the absence of any complexes, which is referred to as “control”. As shown in EIS spectrum of control, semi-circle corresponding to the presence of coating was not observed (Fig. 5a). In the case of Fe-catechol system, a semi-circle corresponding to the presence of resistor-capacitor (RC) circuit in the coating combining with an inclined line corresponding to the Warburg impedance was observed in EIS spectrum (Fig. 5b). This result indicates that coating could be formed in Fe-cat system. In the case of Fe-Ti-cat system, EIS spectrum also showed a clear semi-circle but the Warburg impedance was not observed (Fig. 5c). Under the conditions investigated in this study, both Fe-cat and Fe-Ti-cat systems created passivating coatings based on the presence of RC circuit (Figs. 5b and 5c).

To compare the electrochemical properties of the coatings formed in Fe-cat and Fe-Ti-cat systems, EIS spectra were fitted with two equivalent circuit (EC) models: (i) a model consisting of solution resistance (R_s) in parallel circuit configuration to a capacitance (constant phase element (CPE), Q_f) and resistance (R_d), and Warburg impedance (W_s) for EIS of Fe-cat system, and (ii) a model composed of solution resistance (R_s) in a parallel circuit configuration to a capacitance (CPE, Q_f) and resistance (R_d) for EIS of Fe-Ti-cat system (see the insets in Fig. 5). R_d and CPE (Q_f) refer to net resistance of coating "defect" areas and the capacitance of coating, respectively, while W_s represents for Warburg short corresponding to the diffusion with transmissive boundary. The EC parameters calculated by fitting EIS spectra using EC models are summarized in Table 2. The Z_{Re} value at the starting point of each semicircle indicates solution resistance, and a semi-circle shape indicates the impedance of coating composed of both resistance and capacitance (Yuniati et al., 2015). The radius of the semi-circle represents the resistance of the coating. As shown in Table 2, R_d value of the coating formed in Fe-Ti-cat system was around 1200 Ω, which is about five-fold higher compared with the R_d value measured in Fe-cat system, indicating that coating with higher resistance was formed in Fe-Ti-catechol solution.

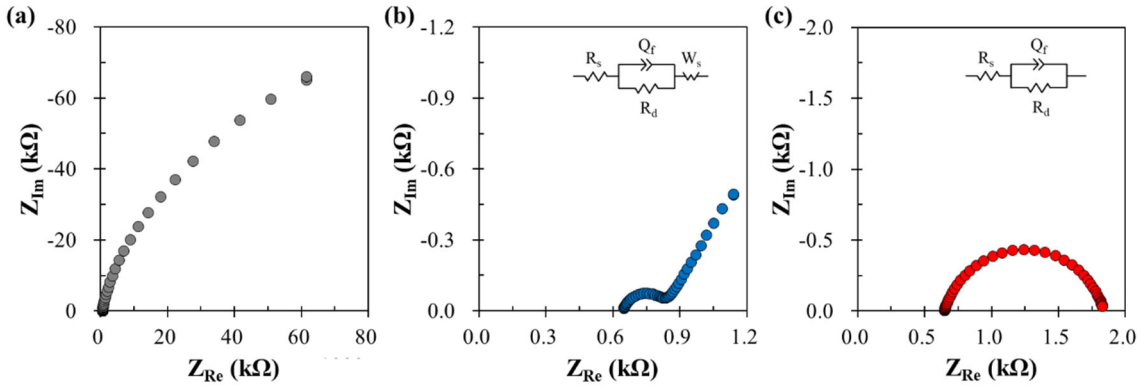

Fig. 5. Nyquist plots of EIS for Pt electrode pretreated by anodic polarization at 0.8 V for 1 h in solutions containing (a) no complex, (b) Fe-catechol, and (c) Fe-Ti-catechol. Note that insets refer to EC models for fitting the EIS data and scales of the plots are different.

Table 2. EC parameters obtained by fitting EIS spectra with EC models (Fig. 5).

	R_s (Ω)	R_d (Ω)	Q_f-T	Q_f-P	W_s-R (Ω)	W_s-T	W_s-P
Fe-cat	652	237	5.33×10^{-5}	0.80	1497	6.52	0.70
Fe-Ti-cat	647	1199	3.71×10^{-5}	0.74	–	–	–

Note that "–" indicates parameters are not applicable to the EC model.

The redox properties of the coatings formed by Fe-cat and Fe-Ti-cat systems were also evaluated by CV. As shown in Fig. 6, a cyclic voltammogram of Pt electrode pretreated by Fe-catechol system shows that during cathodic sweep, a clear cathodic peak (C_1) centered at –0.3 V appeared, which indicate that Fe^{III}-oxyhydroxide coating was reduced as follows:

$$Fe(OH)_3 + e^- \rightarrow Fe(OH)_2 + OH^- \quad (14)$$

A succeeding anodic sweep showed a large anodic peak (A_1) observed at 0.5 V corresponding to the anodic reaction of $Fe(OH)_2$ as illustrated in Eq. 15.

$$Fe(OH)_2 + OH^- \rightarrow Fe(OH)_3 + e^- \quad (15)$$

However, when Pt electrode was pretreated by Fe-Ti-catechol system, anodic/cathodic behaviors were greatly changed; that is, both anodic and cathodic currents were dramatically decreased, indicating that the coating formed by Fe-catechol Ti-catechol complexes was more electrochemically inert than that formed by Fe-catechol complex only.

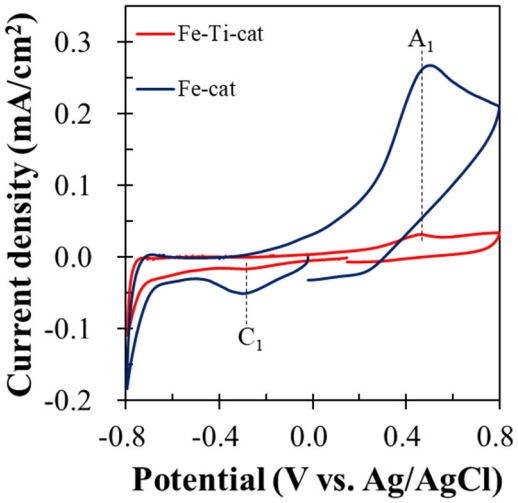

Fig. 6. Cyclic voltammograms of Pt electrode pretreated in Fe-cat and Fe-Ti-cat systems.

4. Conclusions

This study investigated the effects of coexistence of Fe-catechol and Ti-catechol complexes on the complex decomposition and coating formation during CME treatment of pyrite. The findings of this study are summarized as follows:

1. At low concentration of catechol, Ti-catecholate complex was preferentially formed; however, both Fe-catechol and Ti-catechol complexes were formed and stable when enough catechol molecules were present.

2. The precipitation of Fe^{3+} or Ti^{4+} was dramatically accelerated when two complexes coexisted due to simultaneous decomposition of $[Fe(cat)]^{+}$ and $[Ti(cat)_3]^{2-}$.

3. XPS analysis showed that pyrite was coated with a mixture of Fe-oxyhydroxide and Fe_2TiO_5 in the Fe-catechol and Ti-catechol mixture.

4. EIS spectra implied that Fe-catechol and Fe-Ti-catechol systems created coatings based on the presence of semi-circles in Nyquist plots, and the resistance of coating formed by Fe-Ti-catechol system was five-fold higher than that formed by Fe-catechol system.

5. CV results indicated that the coating formed in Fe-Ti-catechol system was more electrochemically inert than that formed in Fe-catechol system.

Acknowledgments

This study was financially supported by the Japan Society for the Promotion of Science (JSPS) grant-in-aid for scientific research (Grant number: JP17H03503 and JP17K12831).

References

Ačai, P., Sorrenti, E., Gorner, T., Polakovič, M., Kongolo, M., de Donato, P., 2009. Pyrite passivation by humic acid investigated by inverse liquid chromatography. Colloids Surf. A 337(1-3), 39-46.

Aikawa, K., Ito, M., Segawa, T., Jeon, S., Park, I., Tabelin, C.B., Hiroyoshi, N., 2020. Depression of lead-activated sphalerite by pyrite via galvanic interactions: Implications to the selective flotation of complex sulfide ores. Miner. Eng. 152, 106367.

An, X., Lan, H., Liu, R., Liu, H., Qu, J., 2017. Light absorption modulation of novel Fe_2TiO_5 inverse opals for photoelectrochemical water splitting. New J. Chem. 41, 7966–7971.

Avdeef, A., Sofen, S.R., Bregante, T.L., Raymond, K.N., 1978. Coordination chemistry of microbial iron transport compounds. 9. Stability constants for catechol models of enterobactin. J. Am. Chem. Soc. 100, 5362–5370.

Baharel, K., Habibi, M.H., 2019. High photocatalytic activity of light-driven Fe_2TiO_5 nanoheterostructure toward degradation of antibiotic metronidazole. J. Ind. Eng. Chem. 80, 292–300.

Cai, M.F., Dang, Z., Chen, Y.W., Belzile, N., 2005. The passivation of pyrrhotite by surface coating. Chemosphere 61(5), 659-667.

Creutz, C., Chou, M.H., 2008. Binding of catechols to mononuclear titanium (IV) and to 1- and 5-nm TiO_2 nanoparticles. Inorg. Chem. 47, 3509–3514.

Davis Jr., R.A., Welty, A.T., Borrego, J., Morales, J.A., Pendon, J.G., Ryan, J.G., 2000. Rio Tinto estuary (Spain): 5000 years of pollution. Environ. Geol. 39, 1107–1116.

Dean, J.A., Lange, N.A., Lange's handbook of chemistry, 15th ed., McGraw-Hill, New York, 1999.

Diao, Z., Shi, T., Wang, S., Huang, X., Zhang, T., Tang, Y., Qiu, R., 2013. Silane-based coatings on the pyrite for remediation of acid mine drainage. Water Res. 47(13), 4391-4402.

Elsetinow, A.R., Borda, M.J., Schoonen, M.A., Strongin, D.R., 2003. Suppression of pyrite oxidation in acidic aqueous environments using lipids having two hydrophobic tails. Adv. Environ. Res. 7(4), 969-974.

Evangelou, V.P., 1995. Pyrite oxidation and its control. CRC press, Boca Raton, FL.

Gazea, B., Adam, K., Kontopoulos, A., 1996. A review of passive systems for the treatment of acid mine drainage. Miner. Eng. 9(1), 23-42.

Grosvenor, A.P., Kobe, B.A., Biesinger, M.C., McIntyre, N.S., 2004. Investigation of multiplet splitting of Fe 2p XPS spectra and bonding in iron compounds. Surf. Interface Anal. 36, 1564–1574.

Ho, G.D., Tabelin, C.B., Tangviroon, P., Tamamura, S., Igarashi, T., 2021. Effects of cement addition on arsenic leaching from soils excavated from projects employing shield-tunneling method. Geoderma 385, 114896.

Hornn, V., Ito, M., Shimada, H., Tabelin, C.B., Jeon, S., Park, I., Hiroyoshi, N., 2020a. Agglomeration–Flotation

of Finely Ground Chalcopyrite Using Emulsified Oil Stabilized by Emulsifiers: Implications for Porphyry Copper Ore Flotation. Metals 10(7), 912.,

Hornn, V., Ito, M., Yamazawa, R., Shimada, H., Tabelin, C.B., Jeon, S., Park, I., Hiroyoshi, N., 2020b. Kinetic Analysis for Agglomeration-Flotation of Finely Ground Chalcopyrite: Comparison of First Order Kinetic Model and Experimental Results. Materials Transactions 61(10), 1940-1948.

Horner, L., Geyer, E., 1965. Zur Kenntnis der o-Chinone, XXVII: Redoxpotentiale von Brenzcatechin-Derivaten. Chem. Ber. 98, 2016–2045.

Huminicki, D.M., Rimstidt, J.D., 2009. Iron oxyhydroxide coating of pyrite for acid mine drainage control. Appl. Geochem. 24(9), 1626-1634.

Huyen, D.T., Tabelin, C.B., Thuan, H.M., Dang, D.H., Truong, P.T., Vongphuthone, B., Kobayashi, M., Igarashi, T., 2019a. The solid-phase partitioning of arsenic in unconsolidated sediments of the Mekong Delta, Vietnam and its modes of release under various conditions. Chemosphere 233, 512–523.

Huyen, D.T., Tabelin, C.B., Thuan, H.M., Dang, D.H., Truong, P.T., Vongphuthone, B., Kobayashi, M., Igarashi, T., 2019b. Geological and geochemical characterizations of sediments in six borehole cores from the arsenic-contaminated aquifer of the Mekong Delta, Vietnam. Data in Brief, 104230.

Igarashi, T., Hererra, P.S., Uchiyama, H., Miyamae, H., Iyatomi, N., Hashimoto, K., Tabelin, C.B., 2020. The two-step neutralization ferrite-formation process for sustainable acid mine drainage treatment: Removal of copper, zinc and arsenic, and the influence of coexisting ions on ferritization. Sci. Total Environ. 715, 136877.

Johnson, D.B., Hallberg, K.B., 2005. Acid mine drainage remediation options: a review. Sci. Total Environ. 338(1-2), 3-14.

Kefeni, K.K., Msagati, T.M., Mamba, B.B., 2015. Synthesis and characterization of magnetic nanoparticles and study their removal capacity of metals from acid mine drainage. Chem. Eng. J. 276, 222-231.

Khummalai, N., Boonamnuayvitaya, V., 2005. Suppression of arsenopyrite surface oxidation by sol-gel coatings. J. Biosci. Bioeng. 99(3), 277-284.

Kumagai, N., Hiraki, T., Pal, U.B., Kasai, E., Nagasaka, T., 2018. A new approach to processing rutile from

ilmenite ore utilizing the instability of pseudobrookite. Metall. Mater. Trans. B 49, 2278–2284.

Lee, D., Baltazar, V.U., Smart, T.J., Ping, Y., Choi, K.-S., 2020. Electrochemical Oxidation of Metal–Catechol Complexes as a New Synthesis Route to the High-Quality Ternary Photoelectrodes: A Case Study of Fe_2TiO_5 Photoanodes. Appl. Mater. Interfaces 12(26), 29275–29284.

Li, J., Kosugi, T., Riya, S., Hashimoto, Y., Hou, H., Terada, A., Hosomi, M., 2016. Potential for leaching of arsenic from excavated rock after different drying treatments. Chemosphere 154, 276–282.

Li, X., Hiroyoshi, N., Tabelin, C.B., Naruwa, K., Harada, C., Ito, M., 2019a. Suppressive effects of ferric-catecholate complexes on pyrite oxidation. Chemosphere 214, 70-78.

Li, X., Gao, M., Hiroyoshi, N., Tabelin, C.B., Taketsugu, T., Ito, M., 2019b. Suppression of pyrite oxidation by ferric-catecholate complexes: An electrochemical study. Miner. Eng. 138, 226-237.

McKibben, M.A., Barnes, H.L., 1986. Oxidation of pyrite in low temperature acidic solutions: Rate laws and surface textures. Geochim. Cosmochim. Acta 50(7), 1509-1520.

Nesbitt, H.W., Muir, I.J., 1994. X-ray photoelectron spectroscopic study of a pristine pyrite surface reacted with water vapour and air. Geochim. Cosmochim. Acta 58(21), 4667–4679.

Opiso, E.M., Maestre, C.V., Aseniero, J.P.J., Tabelin, C.B., Park, I. and Villacorte-Tabelin, M., 2021. Stabilization of small-scale and artisanal gold mine (ASGM) with coal fly ash, palm oil fuel ash, and sugar-mill lime sludge via geopolymerization. Heliyon 7, e06654

Ouyang, Y., Liu, Y., Zhu, R., Ge, F., Xu, T., Luo, Z., Liang, L., 2015. Pyrite oxidation inhibition by organosilane coatings for acid mine drainage control. Miner. Eng. 72, 57-64.

Park, I., Tabelin, C.B., Magaribuchi, K., Seno, K., Ito, M., Hiroyoshi, N., 2018a. Suppression of the release of arsenic from arsenopyrite by carrier-microencapsulation using Ti-catechol complex. J. Hazard. Mater. 344, 322-332.

Park, I., Tabelin, C.B., Seno, K., Jeon, S., Ito, M., Hiroyoshi, N., 2018b. Simultaneous suppression of acid mine drainage formation and arsenic release by Carrier-microencapsulation using aluminum-catecholate complexes. Chemosphere 205, 414-425.

Park, I., Tabelin, C. B., Jeon, S., Li, X., Seno, K., Ito, M., Hiroyoshi, N., 2019. A review of recent strategies for acid mine drainage prevention and mine tailings recycling. Chemosphere 219, 588-606.

Park, I., Hong, S., Jeon, S., Ito, M., Hiroyoshi, N., 2020a. A Review of Recent Advances in Depression Techniques for Flotation Separation of Cu–Mo Sulfides in Porphyry Copper Deposits. Metals 10(9), 1269.

Park, I., Tabelin, C.B., Seno, K., Jeon, S., Inano, H., Ito, M., Hiroyoshi, N., 2020b. Carrier-microencapsulation of arsenopyrite using Al-catecholate complex: nature of oxidation products, effects on anodic and cathodic reactions, and coating stability under simulated weathering conditions. Heliyon 6(1), e03189.

Park, I., Higuchi, K., Tabelin, C.B., Jeon, S., Ito, M., Hiroyoshi, N., 2021. Suppression of arsenopyrite oxidation by microencapsulation using ferric-catecholate complexes and phosphate. Chemosphere 269, 129413.

Qiu, X., Liu, M., Hayashi, T., Miyauchi, M., Hashimoto, K., 2013. Solution-based synthesis of pyrite films with enhanced photocurrent generation. Chem. Commun. 49, 1232-1234.

Regue, M., Ahmet, I.Y., Bassi, P.S., Johnson, A.L., Fiechter, S., van de Krol, R., Abdi, F.F., Eslava, S., Zn-Doped Fe_2TiO_5 Pseudobrookite-Based Photoanodes Grown by Aerosol-Assisted Chemical Vapor Deposition. Appl. Energy Mater. 3, 12066–12077.

Satur, J., Hiroyoshi, N., Tsunekawa, M., Ito, M., Okamoto, H., 2007. Carrier-microencapsulation for preventing pyrite oxidation. Int. J. Miner. Proc. 83(3-4), 116-124.

Tabelin, C.B., Igarashi, T., 2009. Mechanisms of arsenic and lead release from hydrothermally altered rock. J. Hazard. Mater. 169, 980–990.

Tabelin, C.B., Igarashi, T., Tamoto, S., 2010. Factors affecting arsenic mobility from hydrothermally altered rock in impoundment-type in situ experiments. Miner. Eng. 23, 238–248.

Tabelin, C.B., Igarashi, T., Tamoto, S., Takahashi, R., 2012a. The roles of pyrite and calcite in the mobilization of arsenic and lead from hydrothermally altered rocks excavated in Hokkaido, Japan. J. Geochem. Explor. 119–120, 17–31.

Tabelin, C.B., Igarashi, T., Yoneda, T., 2012b. Mobilization and speciation of arsenic from hydrothermally altered rock containing calcite and pyrite under anoxic conditions. Appl. Geochem. 27, 2300–2314.

Tabelin, C.B., Basri, A.H.M., Igarashi, T., Yoneda, T., 2012c. Removal of arsenic, boron, and selenium from excavated rocks by consecutive washing. Water Air Soil Poll. 223, 4153–4167.

Tabelin, C.B., Igarashi, T., Yoneda, T., Tamamura, S., 2013. Utilization of natural and artificial adsorbents in the mitigation of arsenic leached from hydrothermally altered rock. Eng. Geol. 156, 58–67.

Tabelin, C.B., Hashimoto, A., Igarashi, T., Yoneda, T., 2014a. Leaching of boron, arsenic and selenium from sedimentary rocks: I. Effects of contact time, mixing speed and liquid-to-solid ratio. Sci. Total Environ. 472, 620–629.

Tabelin, C.B., Hashimoto, A., Igarashi, T., Yoneda, T., 2014b. Leaching of boron, arsenic and selenium from sedimentary rocks: II. pH dependence, speciation and mechanisms of release. Sci. Total Environ. 473–474, 244–253.

Tabelin, C.B., Igarashi, T., Arima, T., Sato, D., Tatsuhara, T., Tamoto, S., 2014c. Characterization and evaluation of arsenic and boron adsorption onto natural geologic materials, and their application in the disposal of excavated altered rock. Geoderma 213, 163–172.

Tabelin, C.B., Veerawattananun, S., Ito, M., Hiroyoshi, N., Igarashi, T., 2017a. Pyrite oxidation in the presence of hematite and alumina: I. Batch leaching experiments and kinetic modeling calculations. Sci. Total Environ. 580, 687-698.

Tabelin, C.B., Veerawattananun, S., Ito, M., Hiroyoshi, N., Igarashi, T., 2017b. Pyrite oxidation in the presence of hematite and alumina: II. Effects on the cathodic and anodic half-cell reactions. Sci. Total Environ. 581-582, 126-135.

Tabelin, C.B., Sasaki, R., Igarashi, T., Park, I., Tamoto, S., Arima, T., Ito, M., Hiroyoshi, N., 2017c. Simultaneous leaching of arsenite, arsenate, selenite and selenate, and their migration in tunnel-excavated sedimentary rocks: I. Column experiments under intermittent and unsaturated flow. Chemosphere 186, 558-569.

Tabelin, C.B., Sasaki, R., Igarashi, T., Park, I., Tamoto, S., Arima, T., Ito, M., Hiroyoshi, N., 2017d. Simultaneous leaching of arsenite, arsenate, selenite and selenate, and their migration in tunnel-excavated sedimentary rocks: II. Kinetic and reactive transport modeling. Chemosphere 188, 444-454.

Tabelin, C.B., Igarashi, T., Villacorte-Tabelin, M., Park, I., Opiso, E.M., Ito, M., Hiroyoshi, N., 2018. Arsenic,

selenium, boron, lead, cadmium, copper, and zinc in naturally contaminated rocks: A review of their sources, modes of enrichment, mechanisms of release, and mitigation strategies. Sci. Total Environ. 645, 1522–1553.

Tabelin, C., Sasaki, A., Igarashi, T., Tomiyama, S., Villacorte-Tabelin, M., Ito, M., Hiroyoshi, N., 2019a. Prediction of acid mine drainage formation and zinc migration in the tailings dam of a closed mine, and possible countermeasures. MATEC Web of Conferences. 268. EDP Sciences, p. 6003.

Tabelin, C.B., Corpuz, R., Igarashi, T., Villacorte-Tabelin, M., Ito, M., Hiroyoshi, N., 2019b. Hematite-catalysed scorodite formation as a novel arsenic immobilisation strategy under ambient conditions. Chemosphere 233, 946–953.

Tabelin, C.B., Silwamba, M., Paglinawan, F.C., Mondejar, A.J.S., Duc, H.G., Resabal, V.J., Opiso, E.M., Igarashi, T., Tomiyama, S., Ito, M., Hiroyoshi, N., Villacorte-Tabelin, M., 2020a. Solid-phase partitioning and release-retention mechanisms of copper, lead, zinc and arsenic in soils impacted by artisanal and small-scale gold mining (ASGM) activities. Chemosphere 260, 127574.

Tabelin, C.B., Corpuz, R.D., Igarashi, T., Villacorte-Tabelin, M., Alorro, R.D., Yoo, K., Raval, S., Ito, M., Hiroyoshi, N., 2020b. Acid mine drainage formation and arsenic mobility under strongly acidic conditions: Importance of soluble phases, iron oxyhydroxides/oxides and nature of oxidation layer on pyrite. J. Hazard. Mater. 399, 122844.

Tabelin, C.B., Park, I., Phengsaart, T., Jeon, S., Villacorte-Tabelin, M., Alonzo, D., Yoo, K., Ito, M., Hiroyoshi, N., 2021a. Copper and critical metals production from porphyry ores and E-wastes: A review of resource availability, processing/recycling challenges, socio-environmental aspects, and sustainability issues. Resour. Conserv. Recycl. 170, 105610.

Tabelin, C.B., Dallas, J., Casanova, S., Pelech, T., Bournival, G., Saydam, S., Canbulat, I., 2021b. Towards a low-carbon society: A review of lithium resource availability, challenges and innovations in mining, extraction and recycling, and future perspectives. Miner. Eng. 163, 106743.

Tamoto, S., Tabelin, C.B., Igarashi, T., Ito, M., Hiroyoshi, N., 2015. Short and long term release mechanisms of arsenic, selenium and boron from tunnel-excavated sedimentary rock under in situ conditions. J. Contam. Hydrol. 175–176, 60–71.

Tatsuhara, T., Arima T., Igarashi, T., Tabelin, C.B., 2012. Combined neutralization-adsorption system for the disposal of hydrothermally altered excavated rock producing acidic leachate with hazardous elements. Eng. Geol. 139–140, 76–84.

Taylor, J., Pape, S., Murphy, N., 2005. A summary of passive and active treatment technologies for acid and metalliferous drainage (AMD). In: 5th Australian workshop on acid drainage, Fremantle, Australia.

Tomiyama, S., Igarashi, T., Tabelin, C.B., Tangviroon, P. and Ii, H., 2019. Acid mine drainage sources and hydrogeochemistry at the Yatani mine, Yamagata, Japan: A geochemical and isotopic study. J. Contam. Hydrol. 225, 103502.

Tomiyama, S., Igarashi, T., Tabelin, C.B., Tangviroon, P. and Ii, H., 2020. Modeling of the groundwater flow system in excavated areas of an abandoned mine. J. Contam. Hydrol. 230, 103617.

Yuniati, M.D., Hirajima, T., Miki, H., Sasaki, K., 2015. Silicate covering layer on pyrite surface in the presence of siliconcatechol complex for acid mine drainage prevention. Mater. Trans. 56(10), 1733-1741.

Zhang, Y.L., Evangelou, V.P., 1998. Formation of ferric hydroxide-silica coatings on pyrite and its oxidation behavior. Soil Sci. 163(1), 53-62.